ORIGINAL RESEARCH ARTICLE

# Reaction Sequences in Flash Smelting and Converting Furnaces: An In-depth View

PEKKA TASKINEN and ARI JOKILAAKSO

Flash smelting and flash converting are mature technologies in copper and nickel sulfide smelting. The sensitivity of operation concerning the furnace design is evident. It is obvious that when two unit operations are carried out in separate spaces in the same furnace, skills related to maintenance of suspension oxidation of fine minerals, fluxing, fluid as well as heat flows and the overall energy balance are required. Despite these fundamental features, the flow-sheet wide understanding of linking the suspension oxidation of sulfides with the subsequent smelting processes in the furnace as well as the chemistry of its off-gas train is largely absent in the scientific literature. This review gives a detailed outlook on the microscale phenomena in flash smelting and flash converting furnaces accumulated during the last decades. It connects their vital features and chemistries with the reaction tendencies and heat fluxes in the different parts and reaction zones of the furnace as well as in the off-gas train from the smelter to the acid plant.

Graphic Abstract

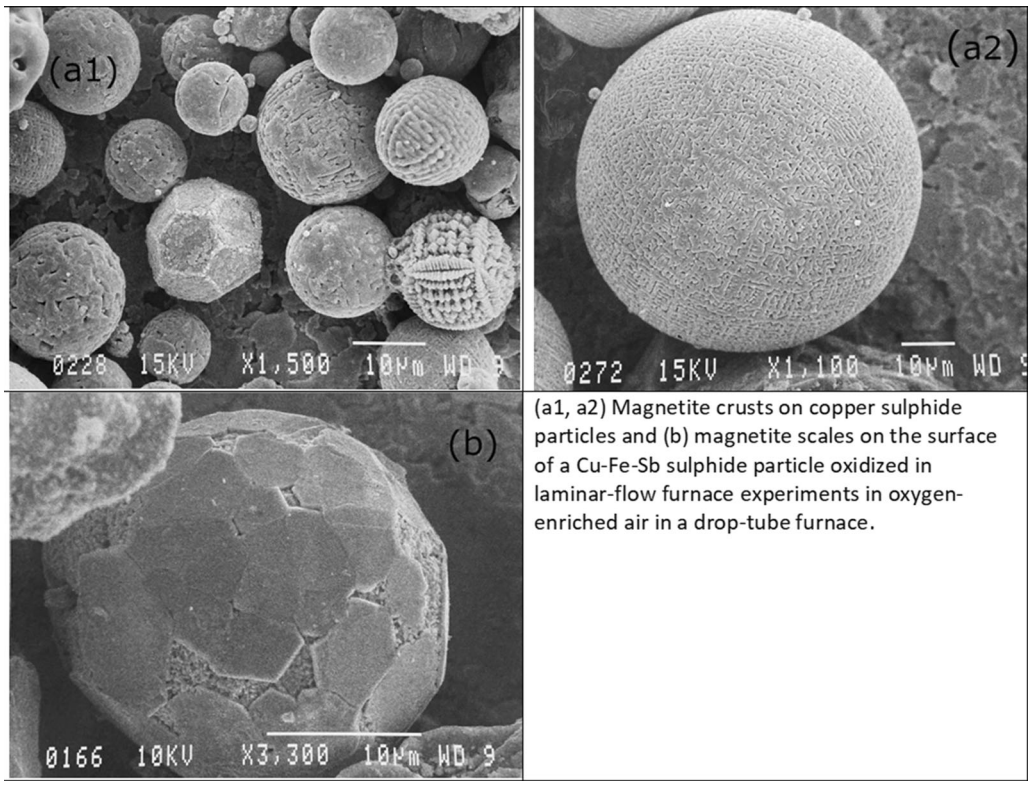


(a1, a2) Magnetite crusts on copper sulphide particles and (b) magnetite scales on the surface of a Cu-Fe-Sb sulphide particle oxidized in laminar-flow furnace experiments in oxygen-enriched air in a drop-tube furnace.

https://doi.org/10.1007/s11663-021-02283-7


PEKKA TASKINEN and ARI JOKILAAKSO are with the Department of Chemical and Metallurgical Engineering, School of Chemical Engineering, Aalto University CHEM, P.O. Box 16100, 00076 Espoo, Finland. Contact e-mail: pekka.taskinen@aalto.fi

Manuscript submitted December 11, 2020, accepted July 15, 2021. Article published online August 10, 2021.

## I. INTRODUCTION

THE flash smelting process has grown to be a major technology in copper and nickel sulfide smelting along with various bath smelting techniques. The attractiveness of the flash smelting is due to, *e.g.*, its high on-line availability, high copper yield, low need of external energy, high sulfur fixing and small carbon footprint.[1] From the metallurgical engineering point of view, this process for sulfide minerals is used as a flash smelting furnace (FSF) and flash converting furnace (FCF) configuration. Its current position and success are a result of the intensive R&D work over the entire period of its existence, for $> 70$ years. The most important milestones of the development trail are the oxygen enrichment adopted in early 1970s, direct-to-blister smelting in the late 1970s and flash converting of solid matte in the 1990s.[2]

The aim of this study is to systematically analyze and quantify the phenomena taking place in this unique smelting vessel. The available information on the thermodynamic and phase equilibria, end point of chemical reactions as well as general features of reaction kinetics including heat and mass transfer, enabling high capacity and smooth operation in each zone, will be reviewed. The limiting factors in the design of FSF and FCF in terms of engineering, throughput and smelting capacity will be discussed based on the fundamental principles of heat generation and dissipation as well as on mass transfer. In this study, the advanced oxide slag database Mtox was used for visualizing the phase equilibria.[3]

## II. SULFIDE SMELTING BY FLASH SMELTING TECHNOLOGIES

The smelter based on the FSF/FCF technology comprises various auxiliary units around the furnace vessel and its immediate functional components: concentrate burner, furnace cooling system and control, tapping holes as well as the on-line and off-line monitoring and advisory systems. Those auxiliary operations include, *e.g.*, raw material handling and drying areas, off-gas heat recovery and flue dust collection and treatment facilities, slag cleaning and sulfuric acid making for sulfur fixation[4]; see Figure 1.

The extensive literature about the flash smelting process since the 1950s has mainly concentrated on overall chemistries of material flows in the furnace and the numerous equipment issues on the furnace and plant level.[5–9] Various descriptions of FSF and FCF reaction chemistry and its sequences in suspension have been given in several textbooks and reviews with a general scope,[4,10] as if they were globally valid within the entire furnace space. The situation has not improved since the detailed modeling studies on the suspension reactions and heat transfer with industrial and laboratory scale data already being published some time ago, as concluded in our recent review.[11] Their focus was on the reaction shaft (RS) fluid flows, heat transfer and its chemical processes using initially 1D in-house codes.[12–14] Based on that fundamental research, many advanced CFD-based (computational fluid dynamics) codes are today in routine use in various development and engineering groups.[15,16]

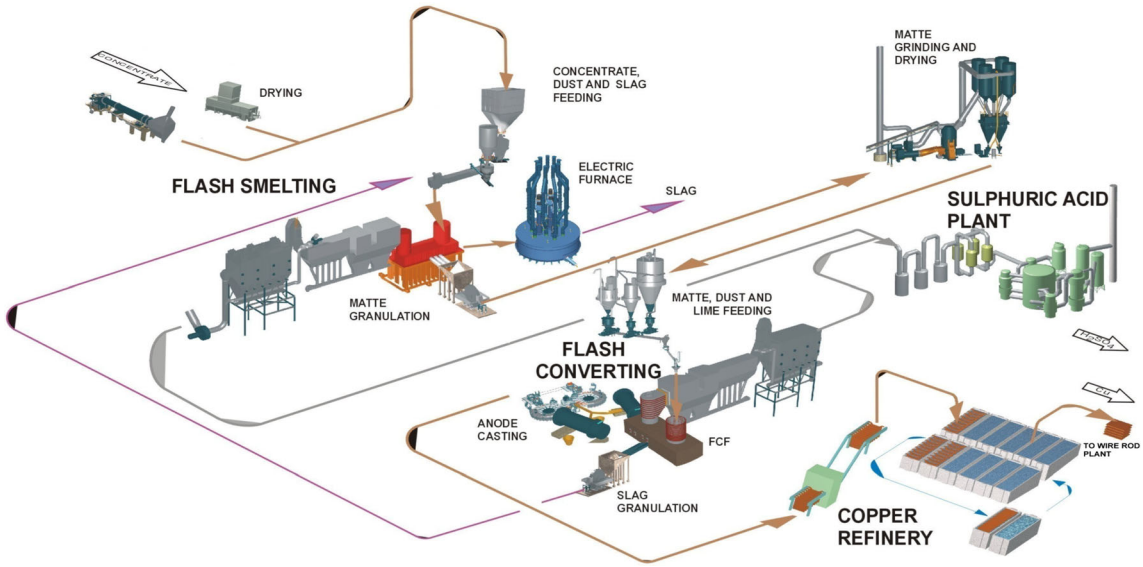


Fig. 1—A simplified flow sheet and the main units of a 'double-flash' copper smelter with a flash smelting furnace for concentrate smelting and a flash converting furnace for continuous solid matte converting to blister copper. Reproduced with permission from Metso-Outotec©.

The FSF for sulfide concentrate smelting to matte and the FCF for solid matte converting to blister copper can be divided functionally into three separate zones that interact with each other quite modestly and where the chemical reactions are exceptionally localized because of the characteristic local vessel geometries and their specific lead times for the material flows.

The fundamental reason allowing the separation of the furnace vessels of FSF and FCF into three functional zones with very little feedback between them is the unique suspension oxidation step taking place entirely in the reaction shaft. The essentially complete phase separation between the condensed phases in the settler finalizes that the leading process off-gas stream is in the front end of the settler (post oxidation step) to uptake shaft and further to gas cleaning. The fact that the process off-gas always contains some flue dust carry over (about 5 wt pct of the dry feed) does not violate the above pattern chemically or in terms of the total heat balance of the furnace.[10] Thus, the matte and slag making processes in the settler do not have any kind of interactions with the reaction shaft (RS) oxidation processes, except the continuous flow of oxidized and hot feed mixture suspension entering the settler and forming its settler products as well as the gas phase.

When the slag and sulfide matte are formed on the top layer of the settler bath surface below the RS,[8,17,18] the specific reaction interface area against the gas flow shrinks at this moment by several orders of magnitude, thus significantly limiting the gas–slag processes and slowing down their reaction rates.

## III. REACTION SHAFT

The feed mixture of fine sulfide concentrates, secondary materials and fluxes are weighed and their flow rate synchronized accurately with the oxygen-enriched process air before distribution evenly in the cross section of the vertical RS. The lead or flight time of the solids in the RS of a typical height of 6 to 10 m is about 2 to 3 seconds. Thus, the feed rates of gas and solids must match very precisely for the stable smelting operation and timewise steady formation of the matte and slag assays. To achieve this strict condition, very high requirements are placed on the design and operation of the concentrate conveying, feed and concentrate burner and their maintenance as well as the feed mixture preparation.

Precise operation of the RS is the key to heat balance of the entire furnace. The gaseous oxygen in air and technical oxygen fed together with the feed mixture are consumed during the flight in RS so that the free oxygen in the process gas on the settler roof level is essentially zero.[19] This is the fundamental difference between Outokumpu/Outotec FSF and the corresponding Canadian (INCO, later Vale Canada) flash smelting furnace.[10] The feed mixture-process gas coupling is poor in the actual sulfide combustion process in the INCO furnace. Thus, the oxidation of sulfides is much less controlled because of a very short flight time; furnace matte of essentially a single composition and a fixed matte grade is produced. The control variable of Outotec FSF/FCF used for adjusting the matte grade produced is the process gas to feed the mixture flow ratio; the oxygen coefficient is the volumetric amount of oxygen ($Nm^3$) needed for one ton of a feed mixture to produce copper matte with a given matte grade.

The present engineering design allows feed rates of > 300 tons per hour through a single concentrate burner (Figure 2). The early generation FSF designs were equipped with several concentrate burners, typically four,[6] but the oxygen and solid flows as well as combustion control in a RS with several burners are very complicated issues and also maintenance intensive solutions.

Fig. 2—A loss-in-weight feeder and large-capacity concentrate burner used commonly in single-burner FSF designs; the lower part of the burner (cooling block and distribution cone) is located in the RS roof and inside the RS. Reproduced with permission from Metso-Outotec©.

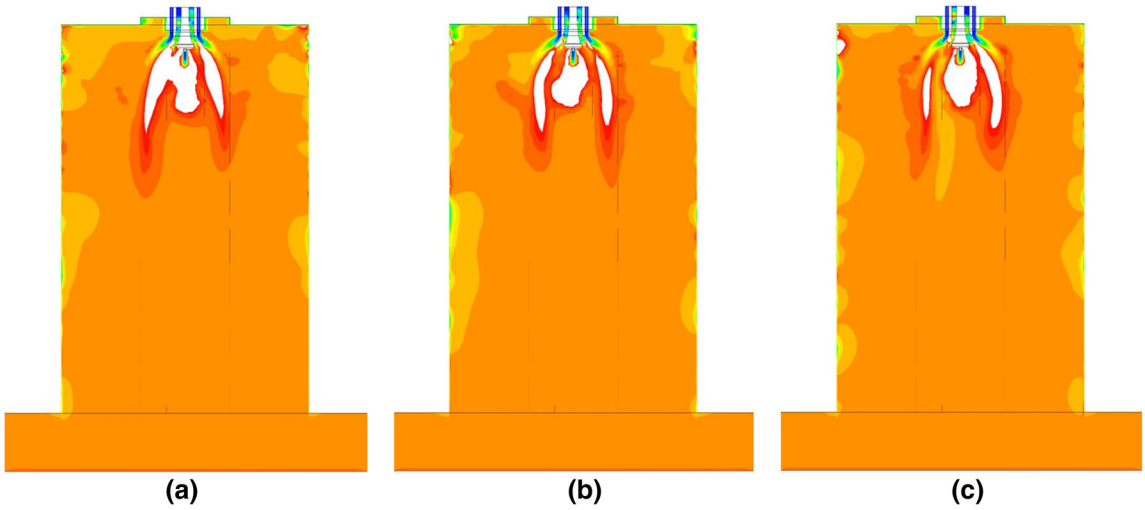


Fig. 3—CFD temperature profiles of a RS centerline section with different air amounts fed through the horizontal channels of concentrate burner distribution cone: (*a*) a special case with decreased distribution air (1500 $Nm^3/h$), (*b*) base case of nominal distribution air (1600 $Nm^3/h$) and (*c*) a special case with increased distribution of air (1700 $Nm^3/h$). Increased amount of distributed air led to a somewhat wider and shorter flame. With low-medium distribution air, the flame width was practically the same. With a high-medium distribution air amount, the flame length was the same, whereas the length of the flame was longer with less air distribution. Reproduced with permission from Metso-Outotec©.

### A. *Heat Transfer in the RS*

The cold or pre-heated process gas and sulfide extract heat from the hot RS walls and from the cloud of combusting suspension, which has reached a high temperature, and ignite in the upper parts of the RS. Individual mineral grains reach their ignition temperatures at certain heights of the RS[20,21] and are combusted in a very short time interval (of the order of magnitude of 10 ms). The computed temperature profiles of a RS with three different distribution air flow rates are shown in Figure 3, indicating the highest temperature area of the combusting suspension.

During the oxidation process, temperatures of individual particles rise much above the targeted smelting temperature,[22,23] depending on the flight time and available oxygen in the surrounding atmosphere. This is also a key requirement for effective heat transfer in the RS suspension between hot particles and cold gas, and the maintenance of heat balance in the furnace, which allows autogenous smelting without external fuel. The very high particle temperature has been evident since the early years of flash smelting operations, when no oxygen enrichment was used, as the flue dust was noticed to enrich with copper compared to iron.[24] It is also an indirect indication of peak temperatures close to the boiling point of copper (2582 °C)[25,26] in particles during their combustion. This has been further discussed by Shook *et al.*[27] in their work of developing a mathematical model of chalcocite particle combustion.

The feed mixture normally enters the RS at the ambient temperature of the plant. The cylindrical wall of the RS can be assumed to be at around 1200 °C as a layer of the feed material deposits on it, and it is in dynamic balance with the heat flux through the wall. It remains at the melting-solidifying temperature of the slag, which is between 1100 °C and 1200 °C.[28,29] In the upper part of the RS, gas is also circulating and swirling; consequently, hot gas from the lower part of the mix with the new process gas stream enters the furnace with the feed mixture.[30]

The particles gain heat is from the hot gas–solid suspension cloud below the concentrate burner and from the surrounding walls by convection and thermal radiation.[31] As the ignition temperatures of sulfidic concentrate particles are between 400 °C and 800 °C,[32] they reach their ignition temperature very quickly and oxidize rapidly. Simultaneous ignition of millions of particles in typical 2 to 5 ton/min feed rate creates a very hot gas suspension cloud, which radiates energy to the surroundings, heating up the gangue, flux and dust particles of the feed mixture and maintains heat balance of the RS.

### B. *Reactions of the Main Sulfides in RS*

During the short heat-up period and prior to ignition in the upper half of RS, the sulfide minerals undergo solid-state oxidation reactions where iron diffuses selectively to surfaces of the sulfide minerals and magnetite

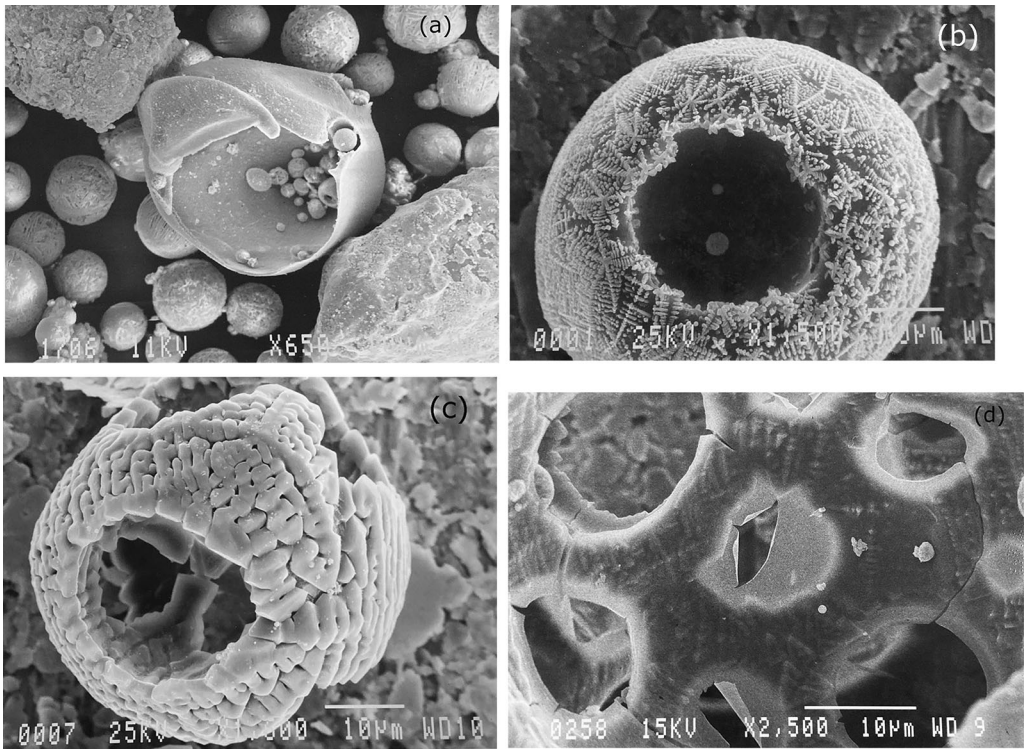


Fig. 4—Oxidation products of chalcopyrite particles after direct quenching in water in laminar flow furnace experiments: partially reacted sulfide (*a*), molten silicate particle (*b*) and drained cenospheres (*c*, *d*).

($Fe_3O_4$) formation takes place.[20,33,34] This initial, very fast oxidation step generates solid magnetite scales on the iron-depleted sulfide particles (see Figure 4), which can be written as:

$$3[Fe]_{sulfide} + 2O_2(g) = Fe_3O_4(s). \quad [1]$$

After that, the actual sulfide combustion reactions occur between the iron-depleted residual sulfide minerals and gaseous oxygen in the surrounding atmosphere. They also include thermal decomposition processes for sulfides, such as dissociation of pyrite and chalcopyrite.[35] In these oxidation sequences, temperature of an individual particle rises much above that of the process gas (1300 °C to 1350 °C) and typically exceeds the melting point of magnetite (≈ 1590 °C,[36]).

The oxidation processes produce a large variety of oxidation degrees to the industrial sulfide concentrate, depending on the mineral and its size, which range from sulfur-depleted matte to metal and further to full oxidation. This can be clearly seen in the oxidation products of a non-classified copper concentrate treated in a drop-tube furnace[33,37] in oxygen-enriched air in Figure 4. Some cenospheres (Figures 4(c) and (d)) have been drained and are hollow without any low-melting sulfide residue in the core.

The overall oxidation reaction in the gas–solid suspension and the average degree of sulfide combustion of chalcopyrite and bornite in the RS and the formation of magnetite crusts can be written as:

$$2CuFeS_2 + (4-x)O_2(g) = [Cu, Fe_x]_2S + (2-2x)FeO + 3SO_2(g) \quad [2]$$

$$Cu_5FeS_4 + \left(2 - 2\tfrac{1}{2}x\right)O_2(g) = 5/2[Cu, Fe_x]_2S + (1-5x)FeO + 1\tfrac{1}{2}SO_2(g) \quad [2']$$

$$3FeO + \tfrac{1}{2}O_2(g) = Fe_3O_4 \quad [3]$$

where x, related to the matte grade produced in the furnace, can be used for estimating the total heat generation and differences of gas volumes before and after reactions in the suspension oxidation. Reactions [2] and [3] as well as the degree of oxygen enrichment are correlated with the produced matte grade, which affects the slag's ferric oxide or 'magnetite' concentration in the slag at a fixed fluxing. Reactions [2] and [3] do not consider the detailed mechanism of suspension oxidation of sulfide minerals where magnetite scale is formed on them prior to actual ignition and the main oxidation reactions, as shown in Reaction [1], but they can be used for heat balance calculations. Reaction [2'] 

may also be used when describing the oxidation of iron in the solid copper matte conversion,[38,39] but the reaction kinetics is much slower in FCF because of the lower amount of Fe and S leading to slower ignition and temperature rise of the granulated and ground high-grade matte (≈ 70 wt pct Cu) from the FSF than the natural minerals.

In addition to the main copper mineral oxidation, typical side sulfides of chalcopyrite concentrates and labile sulfur are also combusted in the RS suspension. Their reactions with gaseous oxygen can be written as:

$$FeS_2 + O_2(g) = FeS + SO_2(g) \quad [4]$$

$$S + O_2(g) = SO_2(g) \quad [5]$$

where also the pyrrhotite (FeS) may over-oxidize forming iron oxides (FeO and $Fe_3O_4$) if its particle size is very small. The gaseous sulfur reacts in the RS due to its good mixing and is not carried in elemental form over to the settler and further to the off-gas train.

At high-enough temperatures (> 700 °C), the thermally unstable fractions of the feed mixture, typically sulfates of the flue dust re-circulated to the smelting, are decomposed in RS. Flue dust accounts for typically 5 wt pct of the FSF feed mixture; thus, its sulfates generate a significant amount of pure, gaseous oxygen by thermal dissociation of sulfur trioxide, which can be written as:

$$\begin{aligned} MeSO_4 &= MeO + SO_3(g) \\ &= MeO + SO_2(g) + {}^1\!/_2 O_2(g). \end{aligned} \quad [6]$$

Due to the natural particle size distribution (+ 30 to − 75 $\mu$m),[40] generated by the froth flotation-grinding circuits of sulfide mineral mines, the fine sulfide fraction of the feed mixture is oxidized completely and the coarse fraction may not have reached ignition temperature in the RS when it enters the settler. The reaction sequences described above have been incorporated in the 3D reaction shaft CFD multi-physics model for engineering and design purposes.[15,30] Reactions [2] and [3] also indicate a minor decrease in the $SO_2(g)$ amount with reference to the oxygen enrichment adopted. Its concentration in off-gas, therefore, increases when the oxidation reactions proceed and the matte enriches, depending on the matte grade produced and the mineralogy of the copper concentrate mixture.

In industrial conditions, the small particle size fractions of the sulfide concentrate ignite first, reacting thus in an oxygen-rich process gas, where oxygen has not yet been consumed by combustion reactions and no $SO_2$ has depleted it. They over-oxidize forming metallic copper and oxides. This means that the oxidized suspension product of the feed mixture entering the settler from the RS is very heterogeneous as far as chemistry, degree of oxidation and mineralogy of the individual particles are concerned. Thus, the final sulfide matte and furnace slag are generated in the settler, and the oxygen needed for those processes has already been extracted in the RS from the process gas and transferred to the condensed particulates and to the furnace off-gas as $SO_2$. At the same time, the process gas has been heated by the condensed particles and their oxidation enthalpies to the desired temperature for the settler processes.

### C. *Reactions of the Impurity Sulfides*

The minority sulfides in the feed mixture, typically, *e.g.*, the impurity carriers sphalerite (ZnS), tennantite ($Cu_{12}As_4S_{13}$), tetrahedrite ($(Cu,Fe)_{12}Sb_4S_{13}$), arsenopyrite (FeAsS) and gersdorffite (NiAsS), are less reactive in suspension oxidation than the main copper minerals, and their ignition temperatures are higher than that of chalcopyrite.[20,33] As they typically exist as non-liberated grains together with the main copper minerals and iron sulfides, the trace sulfides mainly oxidize in the RS simultaneously with chalcopyrite, and the reactions are triggered by the ignition of the main mineral. Their stoichiometric oxidation reactions, with selected minerals of arsenic, antimony and zinc as examples, can be written as:

$$ZnS + O_2(g) = Zn(g) + SO_2(g) \quad [7]$$

$$\begin{aligned} Cu_{12}As_4S_{13} + 7O_2(g) = {} & 6Cu_2S + AsS(g) \\ & + 1{}^1\!/_2 As_2O_3(g) + 6SO_2(g) \end{aligned} \quad [8]$$

$$\begin{aligned} (Cu,Fe)_{12}Sb_4S_{13} + 7O_2(g) = {} & 3Cu_2S + 6FeO \\ & + 2Sb_2S_3(g) + 3SO_2(g) \end{aligned} \quad [9]$$

$$FeAsS + {}^3\!/_4 O_2(g) = FeS + {}^1\!/_2 As_2O_3(g) \quad [10]$$

$$\begin{aligned} NiAsS + {}^{13}\!/_{12}\, O_2(g) = {} & {}^1\!/_2 As_2O_3(g) + {}^1\!/_3 Ni_3S_2 \\ & + {}^1\!/_3 SO_2(g). \end{aligned} \quad [11]$$

The standard states of the products in Eqs. [7] through [11] have been chosen based on their boiling points at typical smelting temperatures.

The equilibrium phase assemblies of oxidation reactions [7], [9] through [11] with stoichiometric amounts of oxygen are shown in Figure 5. The atmosphere of essentially pure $SO_2(g)$ at 0.5 atm was selected for the equilibria, representing conditions in lower RS sections. The calculations were carried out with MTDATA software (vers. 7.1) using the Mtox oxide database.[3,41] The basic difference in the oxidation reactions [7] through [11] is behavior of the condensed phases. When the oxidation products of sphalerite are completely gasified at about 1400 °C, those of, *e.g.*, tetrahedrite and

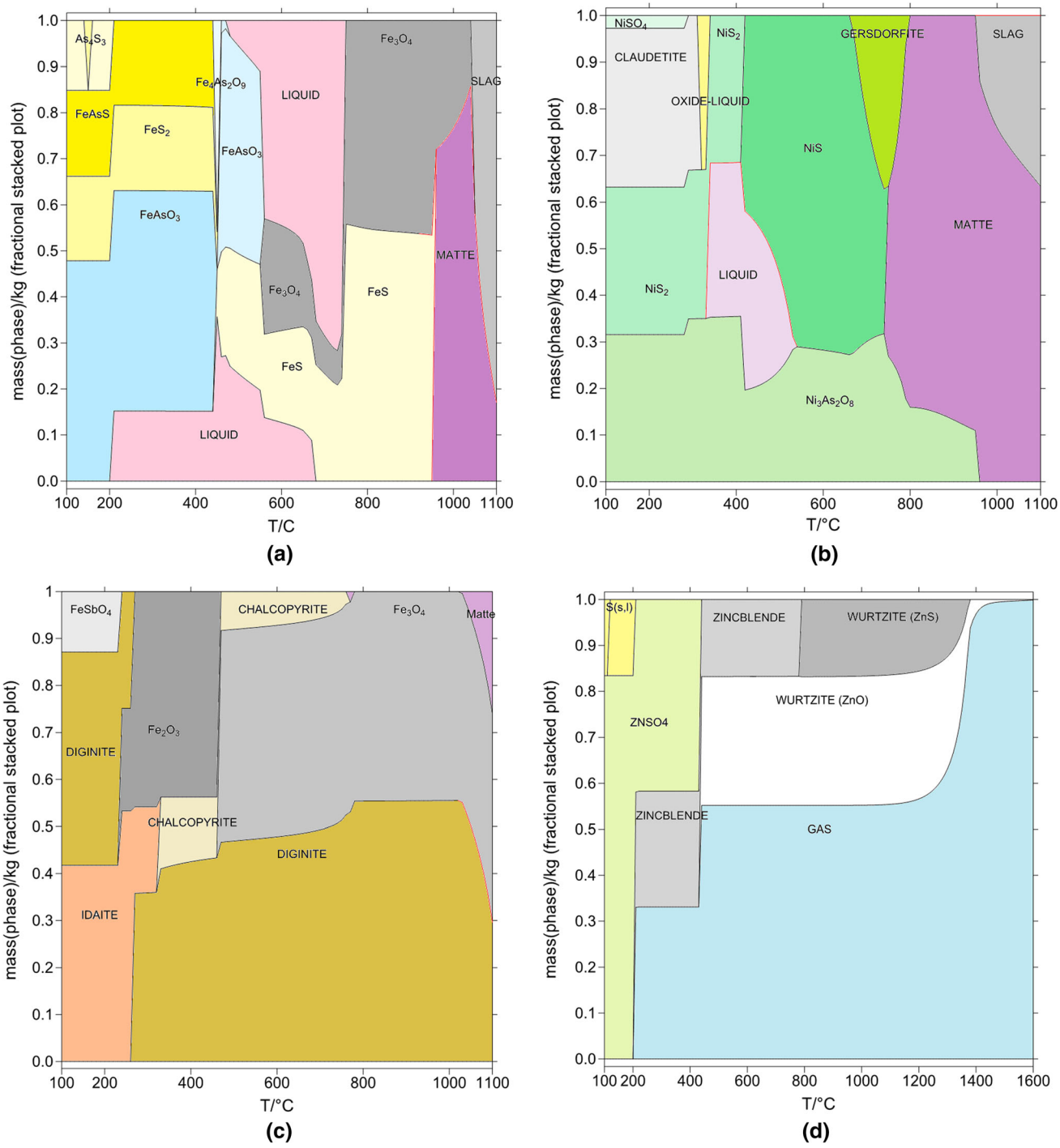


Fig. 5—Equilibrium phase assemblages of the condensed oxidation products of selected impurity element carrier minerals of sulfidic copper concentrates in stoichiometric reactions [7] through [9] through [11] at $p(SO_2) \approx 0.5$ atm: (*a*) FeAsS-$O_2$ equilibria (no gas phase included in a, b and c), (*b*) NiAsS-$O_2$ equilibria, (*c*) $(Cu,Fe)_{12}Sb_4S_{13}$-$O_2$ equilibria and (*d*) ZnS-$O_2$ equilibria (including gas phase); calculated with MTDATA (vers. 7.1) and Mtox database, vers. 8.2[3]

tennantite form a copper sulfide matte stable at very high temperatures.[42] Thus, a fraction of gaseous oxidation products may be captured by the forming sulfide matte, depending on the vapor pressures of arsenic and antimony sulfides and oxides, but for zinc and its carrier sphalerite no such condensed matte phase is formed (Figure 5(d)).

In equilibrium conditions, the As–S–O system forms a low-temperature oxide melt stabilization, according to the Mtox database, in atmospheric conditions between 200 °C and 700 °C. This can be seen in the condensed reaction products of arsenopyrite and gersdorffite (Figures 5(a) and (b)), as a narrow liquid oxy-sulfide domain. The vaporization of $As_2O_3$ from the oxidizing mineral is obviously very rapid, as such molten phase

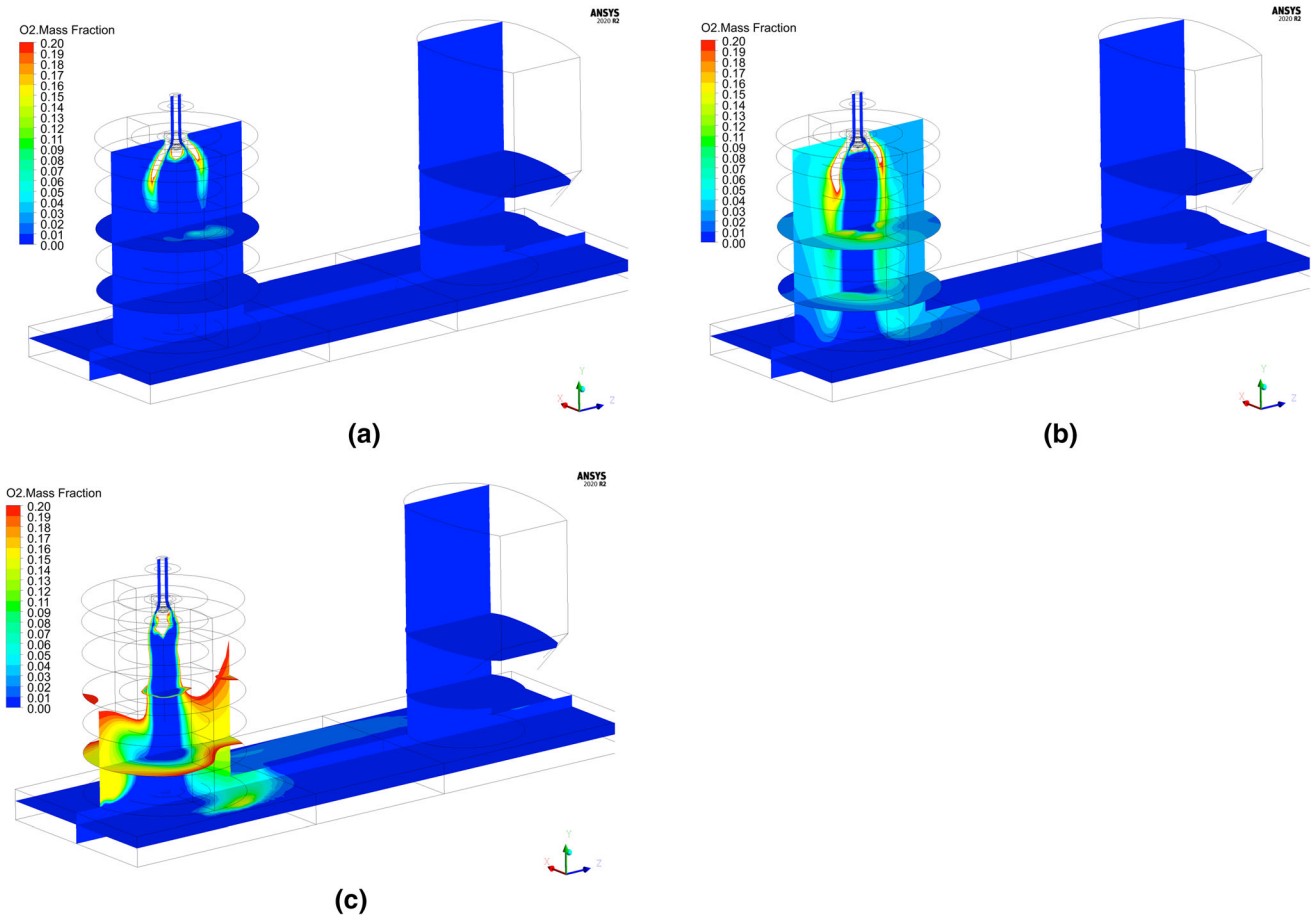


Fig. 6—A CFD comparison of the oxygen concentration distribution profiles in the RS with different feed mixture amounts, compositions and additions of inert material: (*a*) base case of 111 dmtph* feed rate, (*b*) increased feed rate of 130 dmtph and (*c*) feed rate of 140 dmtph, with non-combustive coolant added in the feed mixture. Reproduced with permission from Metso-Outotec©.

has not been found in oxidation experiments of arsenic sulfide or copper-arsenic sulfides.[43,44] The situation may be different with antimony[45] as its vapor pressures are much lower than those or arsenic.

Analogical oxidation reactions can be written for the other impurity sulfides of copper concentrates, such as galena (PbS) and complex Bi–Cu, Cu–Sn as well as Bi–Pb sulfides. There are, however, limited literature data on the behavior of the trace element sulfide particles in the suspension oxidation conditions.

Based on the above analysis and the characteristic feature of the oxidizing RS suspension of large specific surface area, it is evident that most impurity vaporization reactions advance during the oxidation step. Therefore, the evaluation of the vaporization of impurity species in the conditions of matte and slag endpoints is not relevant in FSF/FCF, as pointed out, *e.g.*, by Hahn and Sohn.[12]

### D. *Heat Balance of the Furnace*

The successful operation of FSF from the heat engineering point of view is based on the heat recovery by the cold feed mixture from the combusting suspension in RS, although its flow conditions are close to a plug flow. This is possible when the feed mixture is, *e.g.*, bone dry, and no time is wasted for vaporizing the residual moisture from the feed mixture particles. Vaporization of the residual moisture would slow down the heating rate of the particles, thus moving the ignition point of the sulfides downwards in the RS and shortening the reaction time. The similar effect has agglomeration of the feed mixture taking place during transport, storage and drying of the sulfide concentrates.

An interesting feature of the suspension smelting and operation of the RS in terms of the energy dissipation is the growing enthalpy intensity of the vertical duct of RS where the oxidation reactions take place. Its diameter and thus volume have been within the same order of magnitude over the entire existence of the FSF technology. The significant scale-up in the smelting capacity (from 24 ktpa to $>$ 300 ktpa Cu) has been possible because of the adaption of oxygen-enriched process air in the early 1970s, and even the use of pure oxygen in FCFs and nickel smelting FSFs for low-grade concentrates. It was enabled, *e.g.*, by new furnace cooling technologies and concentrate burner development.[2]

As seen in Figure 3, the ignition and peak temperature of the particles and suspension are in the upper part of the RS. This is also reflected in the oxygen profile of the RS; the computed oxygen mass fractions in the

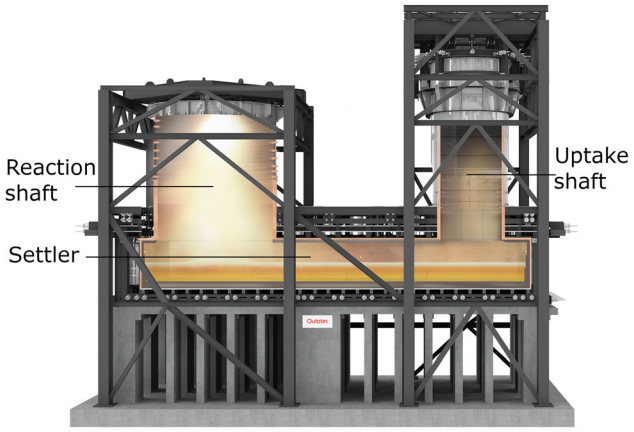


Fig. 7—A schematic drawing of the FSF from the RS end of the settler showing the reaction zone on the settler bath, just below the reaction shaft, responsible for the matte and slag formation processes from the descending, fully oxidized suspension. Reproduced with permission from Metso-Outotec©.

suspension are depicted in Figure 6 in three different raw material cases. First, the base case (a) shows how oxygen is practically speaking completely consumed by the reactions in the upper part of the RS, below the concentrate burner. In the second case (b), a higher feed rate was used resulting in delayed ignition and oxygen consumption. Finally, in the last case of Figure 6(c), a coolant material has been added to the feed and the ignition of the sulfides is significantly slower as the heating; consequently, reaching the ignition temperatures takes a much longer time, leading to a high fraction of residual oxygen in the settler gas phase.

## IV. SETTLER

The oxidized suspension entering the settler has, thus, captured all oxygen added in the furnace as gaseous oxygen of the process gas as well as in form of various solid oxygen carriers, which decompose thermally in the RS.[19] Due to the vessel geometry, the condensed material entering the settler hits the slag surface and simultaneously the gas flow turns horizontally toward the uptake shaft.

The early modeling efforts, based on physical particle density of the suspension,[46] claimed that no particle collisions take place in RS due to its low particle density, thus omitting the possibility of molten slag formation during the oxidation step. This is also supported by the much larger grain size of silica sand, which prevents its rapid heating in flight to temperatures of the iron silicate slag melting domain, above approximately 1150 °C.[47] This pattern has been modified as a result of industrial and pilot scale sampling campaigns[48,49] showing particle growth during fast oxidation processes. Also, agglomeration has been claimed to take place in RS.[50] It together with a sufficient particle temperature is a prerequisite for the slag formation in the suspension and may lead to lowering of the dust carry-over in the

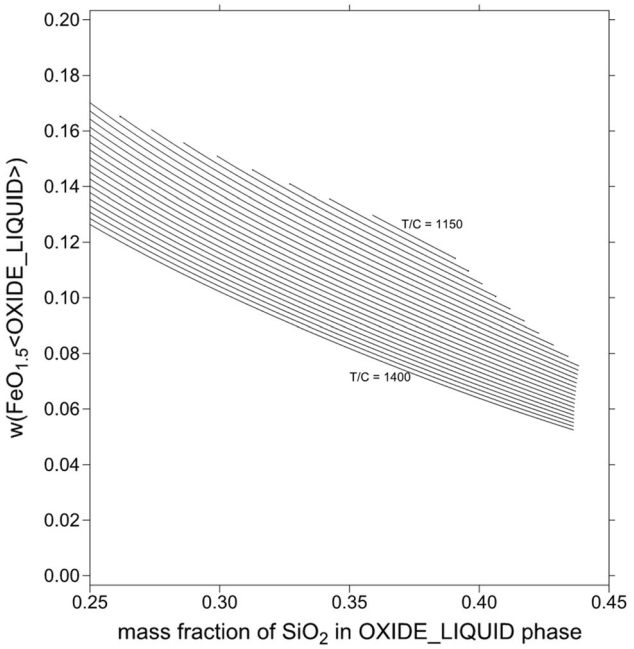


Fig. 8—Solubility of ferric oxide in an iron silicate slag in equilibrium with nickel matte (Ni:Cu = 2.7 w/w) with 5 wt pct Fe in $p(SO_2)$ = 0.5 atm as a function of silica concentration of the slag and temperature (MTDATA and Mtox 8.2 database[3]).

FSF.[51] The sampling in RS is, however, a very sensitive and demanding task, and the results are subject to experimental errors.[52]

### A. *Copper and Nickel Smelting Slags*

The formation of matte and slag takes place on top of the settler bath, immediately below the RS, in a relatively restricted and small area[53]; see Figure 7. The formation of furnace matte and slag starts when the oxidized RS product and molten slag layer on top of the settler meet and allow the growth of matte, dissolution of sand and formation of the slag finally with the reactions between solid iron oxides and the added fluxes. As typical flux of the solid iron oxides is natural silica sand, the reactions of slag formation can be presented as

$$2FeO + vSiO_2 = (FeO)_2 \cdot (SiO_2)_v \quad [12]$$

$$Fe_3O_4 + v\,{}^1\!/_2 SiO_2 = {}^1\!/_2\left[(FeO)_2 \cdot (SiO_2)_v\right] + 2(FeO_{1.5}) \quad [13]$$

where iron silicate (with $v = 1$ denoting fayalite as solid compound) was selected to represent the iron silicate slag. Its composition is in many cases targeted to a fixed level (by the $Fe/SiO_2$ ratio or $SiO_2$ concentration) in the copper smelting by silica additions. Mono-cationic ferric oxide in Eq. [13] represents the dissolving three-valent iron oxide in the slag; see Figure 8. Concentration of dissolved magnetite in the homogeneous iron silicate slags is 1.45 × $w(FeO_{1.5})$.

Silica is industrially used as flux in the copper and nickel matte smelting for the iron oxides forming in the oxidation. Some smelters prefer quartzite (> 99 wt pct $SiO_2$) and some a local silica sand, which typically contains > 10 wt pct potassium feldspar ($KAlSi_3O_8$, an endmember of a wide solution phase) and a smaller fraction of sodium feldspar ($NaAlSi_3O_8$), depending on the bedrock. They, together with gangue of the sulfide concentrate, add some alumina and alkali oxides in the furnace slag, which slightly modify the liquid slag domain at smelting temperatures and, *e.g.*, increase the solubility of silica in the slag.[54]

Since the fundamental review by Schuhmann,[55] data on thermodynamic properties of the matte-slag systems have accumulated significantly, in particular in the 1980s and 1990s, today covering the matte and blister copper smelting.[3,56] Due to the recent intensive investigations on the slag–matte–copper–gas equilibria, the equilibrium properties of the phases and the behavior of, *e.g.*, copper, iron, sulfur and many trace elements, are relatively well known.[42,57–59]

### B. *Mechanism of Slag and Matte Formation*

The constituents of the matte and slag bath in the settler are generated when the over- and under-oxidized feed mixture particles react and mix with the oxidation products of the main feed mixture generated according to Eqs. [2] through [4]. Typical processes occurring in the settler in this localized space of the furnace can be written by simplified single reactions between pure substances, *e.g.*,

$$3Fe_3O_4 + FeS = 10FeO + SO_2(g) \qquad [14]$$

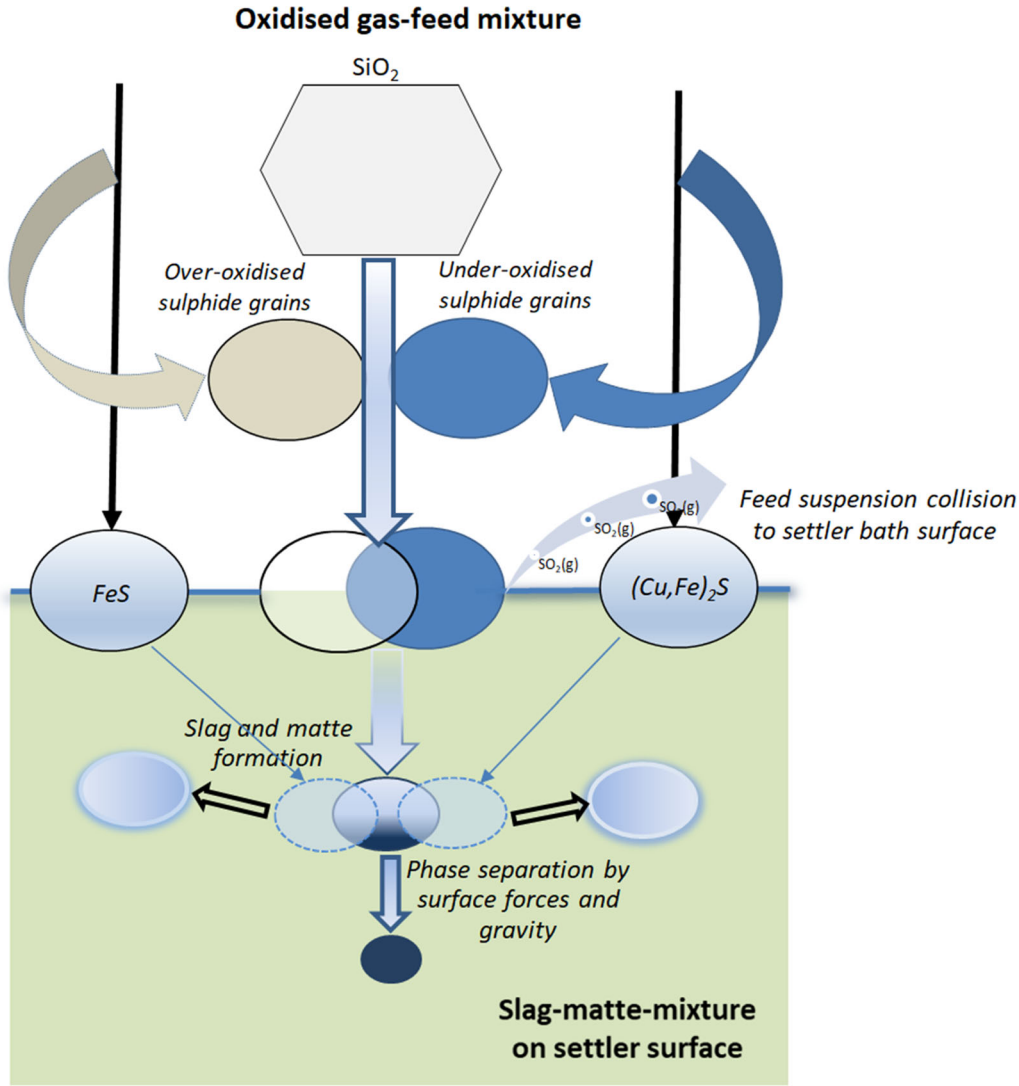


Fig. 9—The schematic mechanism for formation of the matte and slag in FSF on the settler surface below the reaction shaft after suspension oxidation of the feed mixture; the oxidation product is a heterogeneous mixture of oxides and sulfides, which reacts to the essentially final matte and slag assays.

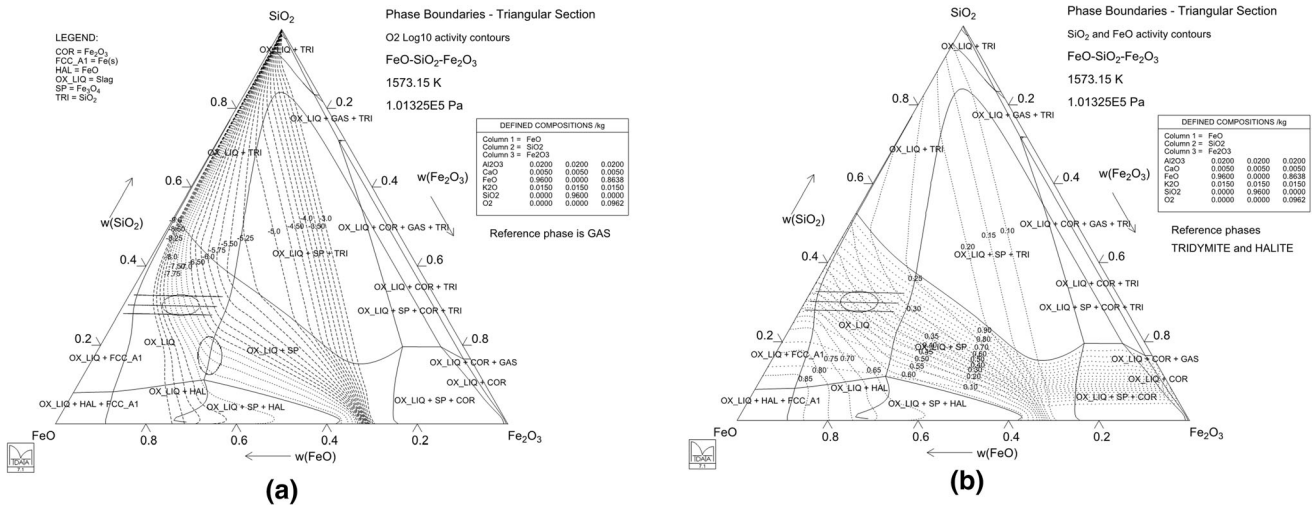


Fig. 10—Isothermal section of the iron-silicate slag system at 1300 °C with (*a*) oxygen iso-activity contours in an iron silicate slag at 1300 °C, (*b*) silica (—) and ferrous oxide (···) iso-activity lines superimposed in a typical slag assay with 2 wt pct $Al_2O_3$, 0.5 wt pct CaO and 1.5 wt pct $K_2O$ at 1300 °C; the dotted lines in (a) show the industrial matte making conditions and its ovals are initial (lower) and end points (upper) in slag making (standard states: $O_2$(g, 1 atm), $SiO_2$(s, tridymite) and FeO(s, halite); MTDATA 7.1 and Mtox 8.2 database.[3]

$$Cu_2O + FeS = Cu_2S + FeO, \qquad [15]$$

but the entire matte and slag formation is controlled by the constraint of forming $SO_2$(g) bubbles in the surface layer on the settler.[17,60] That is the fundamental difference between the bath smelting[59] and the suspension smelting processes. It determines properties of the slag and matte produced in FSF. The mechanism is valid for the slag and blister copper in FCF, where low-S copper melt is produced. In the bath smelting processes, the maximum partial pressure of $SO_2$ is the $p(O_2)$ of the blowing gas,[62] which may be achieved in the last moments of the slag blow in converting when all iron has been oxidized.

The sulfur dioxide partial pressure generated on the slag–matte (slag–blister copper) interface in FSF and FCF is close to the ambient pressure at the smelter site. It is not related with the used oxygen enrichment of process gas or the gaseous $SO_2$(g) partial pressure in the settler gas space. It arises from a straightforward mechanical boundary condition of $SO_2$ bubble formation and from replacement of its volume under the ambient pressure, *e.g.*, in Reaction [14]. Using the properties of the final slag and matte/blister copper we can, thus, write for the molten products in all suspension oxidation processes:

$$O_2(g) + {}^1\!/_2 S_2(g) = 2(O)_{slag} + [S]_{matte} \approx SO_2(g, 1\,atm) \qquad [16]$$

if the smelter is located at sea level. The total pressure is lower at elevated smelter sites and respectively the pressure of $SO_2$ in Reaction [16]. The process can be visualized, as shown in Figure 9.

Reaction [14] is an endothermic process between pure $Fe_3O_4$ and FeS and generates sulfur dioxide partial pressure in excess of 1 atm, depending on the activity of FeO in the slag, at temperatures of the molten iron silicate slags (standard state of ferrous oxide FeO(s, halite)); see Figure 10. The reactions are favored by the dissolving solid silica in the reaction zone which holds the activity of ferrous oxide on a low level. In the tapping slag, in the end point of the settler processes, it is even somewhat lower when the slag is close to silica saturation ($a(SiO_2)$ = 0.6–0.7 referred to solid tridymite). Figure 10(a) also shows the $Fe/SiO_2$ iso-value contours at 1.6, 1.8 and 2.0 (w/w) for the slag studied in the graph (horizontal solid lines). Its orthosilicate composition is at $Fe/SiO_2$ = 1.7, whereas for pure FeO–$Fe_2O_3$–$SiO_2$ slags it is reached at $Fe/SiO_2$ = 1.85.

The boundary condition, Eq. [16], indicates that the oxidation states of the slag and matte represent higher oxygen partial pressures in FSF than those in the bath smelting processes producing the same matte grade.[63] This feature appears from the fact that the properties of copper mattes, such as $p(S_2)$ and [pct S], are essentially constant at each matte grade,[64] but the increased sulfur dioxide partial pressure is compensated by a higher oxygen partial pressure of the system. The increasing oxygen concentration dissolved in matte has a minor impact on this process. As implied by Eq. [16], they have an essentially linear relationship to each other at constant temperature and matte grade.

The micro-scale matte and slag formation processes are not well known or validated experimentally because of the harsh conditions in the industrial furnaces below the RS[65] where sampling in general and getting a representative sample is very challenging. The

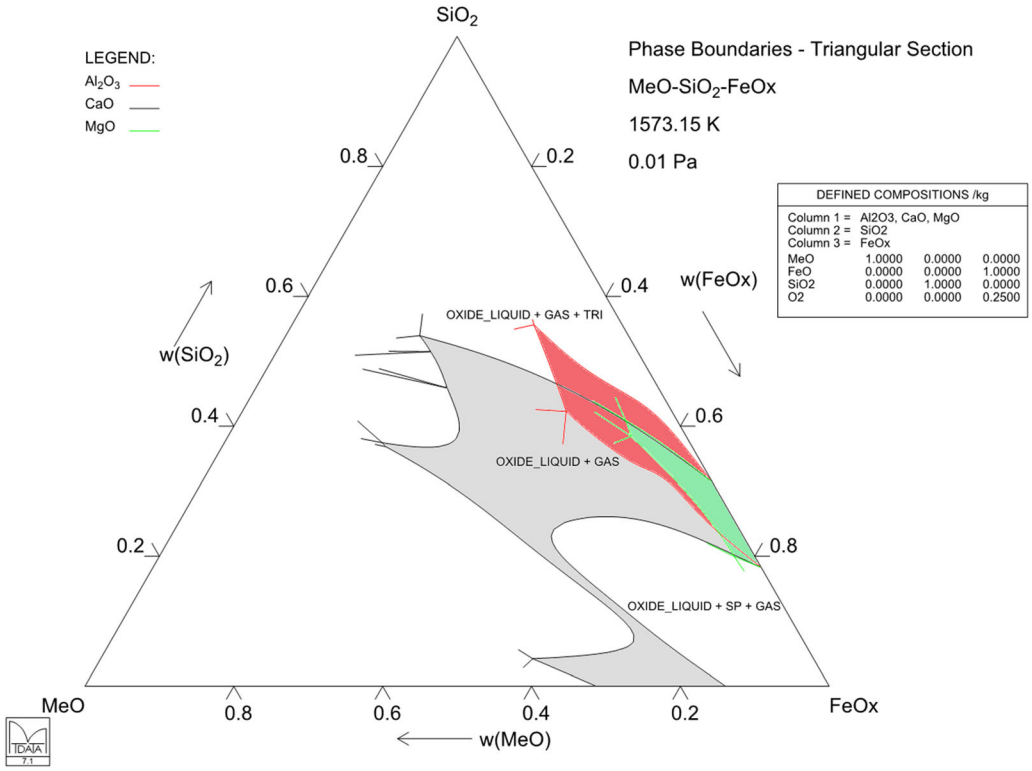


Fig. 11—The effects of $Al_2O_3$, CaO and MgO on the molten slag domain at 1300 °C and $p(O_2)$ = 0.01 Pa ($\approx 10^{-7}$ atm), calculated by MTDATA using the Mtox database vers. 8.2.[3]

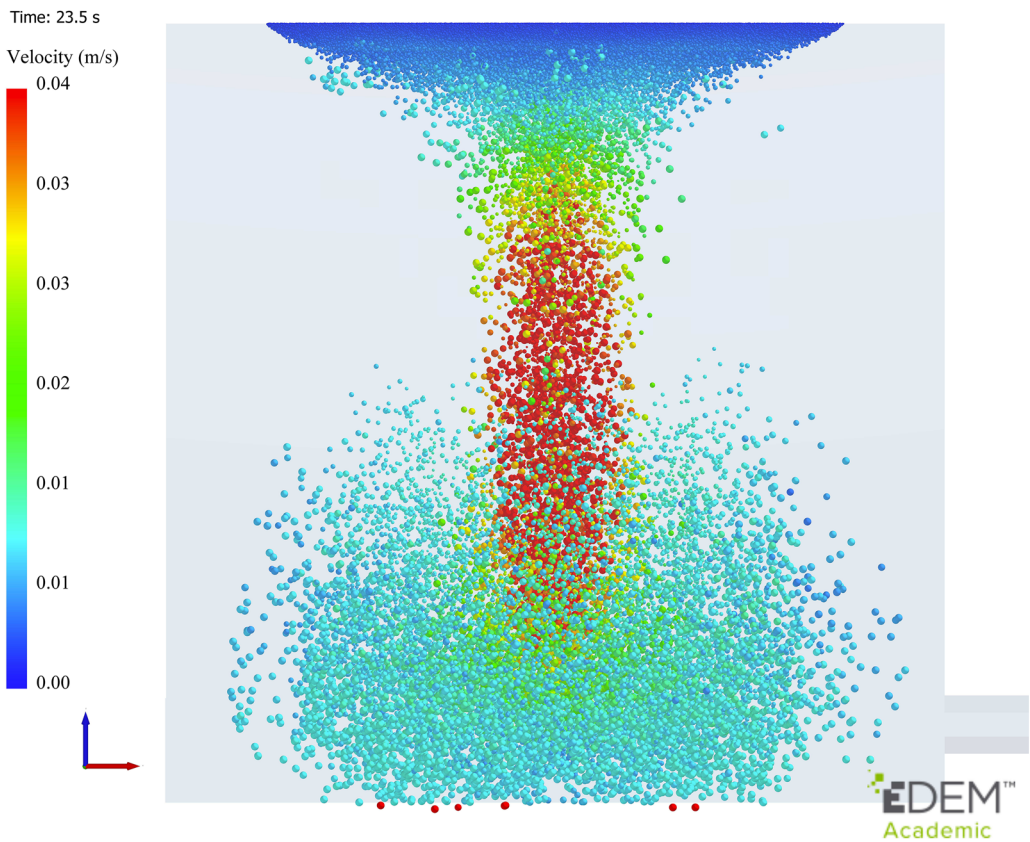


Fig. 12—Descending of a matte droplet swarm through the slag layer in a settler simulated with CFD-DEM.[73]

dissolution of the fluxes and its impact on the physical and chemical properties of the oxide-sulfide melt in settler before the actual slag formation can be estimated from the laboratory scale phase equilibrium and physical property data.

The super-heated suspension product entering the settler is very silica-deficient in most cases, because the coarse silica sand falling because of its small specific surface area and large size enters the settler at a much lower temperature (< 1000 °C) than the rest feed mixture.[66] Thus, the initial melt on the settler surface may contain < 15 wt pct dissolved $SiO_2$ (see Figure 10(b)), and its viscosity, density and surface tension are relatively far from those of the final slag to be tapped from the furnace.

The descending oxidized sulfide fraction of the feed mixture has, therefore, approximately 10 to 20 pct higher density than the average slag, and its viscosity is up to 40 to 50 pct less,[67] which supports the reactions described schematically in Figure 9 and mixing with the bulk slag as well as settling of the matte droplets. A further difference in the slag–matte interactions may be found in the surface and interface energies at low silica-high iron oxide concentrations compared with the tapping slag and matte.

Figure 11 also indicates that at low (< 20 wt pct $SiO_2$) silica concentrations at 1300 °C the slag is saturated with solid magnetite, which will have an impact on the reaction paths in the slag and matte formation process. Potassia, a common minority component in silica sands, along with alumina present in, *e.g.*, feldspar (melting incongruently at 1150 °C ± 20 °C,[68–70] depending on its K-to-Na ratio), has a strong influence on the saturation boundaries of the Fe–O–$SiO_2$ slags. It significantly lowers the melting points of the saturation phases, thus expanding the area of the molten slag domain.

The transition occurring in the process conditions during the initial phase of slag and matte formation and the final slag is depicted in Figures 10(a) through (b). It means a significant difference in terms of silica activity lowering from $a(SiO_2)$ = 0.6–0.7 in the end-slag to about 0.1–0.3 (referred to solid tridymite) at magnetite saturation.

A limited number of modeling studies on the flow conditions of the settler is available in the literature. This is mostly due to severe lack of validation data in the harsh and demanding environment of the settler. The early results[71,72] suggest that the flow pattern generated by the slag tapping from typically two tapping holes is smooth and without strong shear forces for helping droplet growth and settling of matte. More recent coupled CFD-DEM (discrete element method) results show a contraction and a funnel-like flow pattern in the settling droplet swarm descending from the top surface of the settler slag[73] (Figure 12).

The mass flow of the reacted and still reacting feed material from the RS impinges on the slag surface and causes a turbulent and chaotic flow pattern in the slag layer below the RS.[73,74] In the main part of the settler between the RS area and the tap hole(s), the flow is rather stagnant when there is no slag tapping going on. However, when the slag tapping is started, a flow field forms, which is quite symmetric, if the tap hole is on the end wall of the settler, but there is a more unsettled flow pattern with a side wall tapping hole configuration. Furthermore, shortcutting flows can form alongside the walls to the slag tap hole.[73]

There seems to be a three-dimensional area around the slag tap hole, from which the slag flow is sucked to the hole taking; therefore, copper droplets with the flow even below and on the sides of the tap hole level thus increase the copper losses.[70] This is reported also in a physical (water) model and CFD modeling of slag skimming from a rotary holding furnace, where entrainment was found from the copper matte layer below the slag tap hole level because of interfacial tension.[76] Therefore, a slag layer of at least 30 cm was suggested for this furnace type to ensure no matte entrainment.

The details of the flow behavior of the slag layer in the FS settler are still unclear although some modeling results have suggested the main features. What is still most uncertain is the coalescence and settling behavior of matte droplets. The funneling settling behavior has been seen in the two different modeling approaches and both in small scale[73] and full industrial scale CFD models.[74] The latter one indicates, in fact, that the feed material falling to the slag surface forms several contracting funnels as settling channels, taking most of the matte droplets through them down to the matte layer (Figure 13). Therefore, it seems plausible that the droplets escaping these funnels remain unsettled in the slag and are so far away from each other that they cannot coalesce to large enough drops that would settle fast enough and avoid the slag tap hole. This funneling phenomenon still requires physical model validation, which is the next step in the CFD-DEM modeling work by Jylhä *et al.*[73,75]

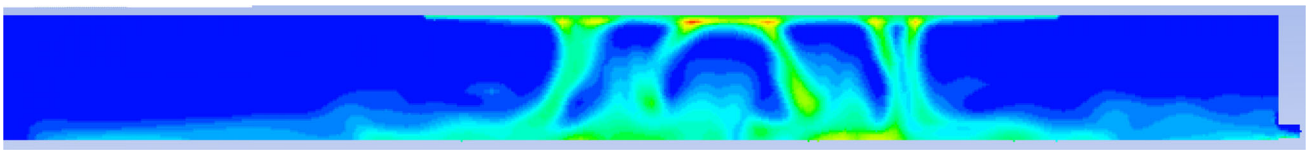

Fig. 13—A centerline cross section of the FSF slag layer below the RS showing several channeled matte settling paths through the slag and toward the matte layer simulated by CFD-DEM.[75]

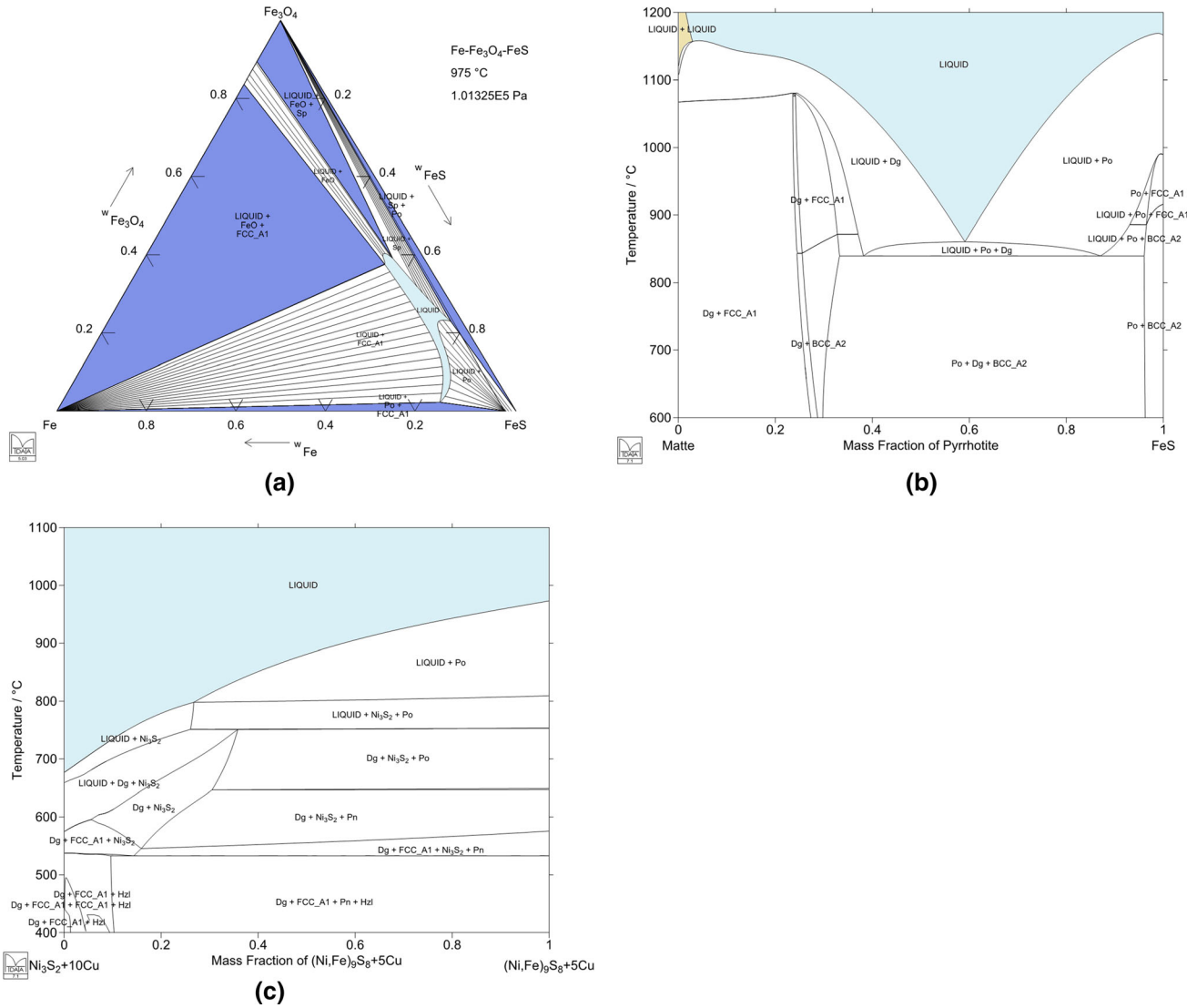


Fig. 14—Selected quasibinary and ternary sections of the key matte systems in copper smelting showing the stability of the molten phase below the smelting temperature of copper sulfide raw materials: (*a*) isotherm of the Fe–$Fe_3O_4$–FeS, (*b*) $Cu_2S$ + 2.5 wt pct Fe–FeS quasibinary section and (*c*) $Ni_3S_2$ + 10 wt pct Cu– $(Ni,Fe)_9S_8$ + 5 wt pct Cu quasibinary section; *Dg* digenite, *Hzl* heazlewoodite, liquid: matte, Cu(l), Pn: pentlandite, Po: pyrrhotite, Sp: spinel ($Fe_3O_4$); calculated using MTDATA and Mtox 8.2. database.[3]

## V. UPTAKE

The uptake shaft (US) of the FSF connects the smelting furnace with the heat recovery or waste heat boiler (HRB). Geometrically, it is located on the extension of the FSF centerline, or it may turn 90 deg angle from it.

The reactions in the uptake shaft are meant to actively control the composition and properties of the flue dust entering the heat recovery boiler and the smelter gas train. Due to the much higher particle temperatures post ignition than the process gas, high-vapor pressure substances are effectively vaporized in the lower half of the RS and transferred to the process gas as described earlier. Those gaseous molecules together with the finest flue dust fractions do not follow the streamlines of the condensed particles to the settler bath. They create the fine fraction of the generating flue dust along with the coarse, mechanically entrained particles from the settler when the off-gas cools down in the off-gas train.

The US design as a vertical duct also acts as a classifier for the flue dust and descends the largest particle size fractions back to the top of the settler products.

There are a few trace elements in the copper sulfide concentrates which form oxides and sulfides with boiling points much below the settler temperatures of 1250 °C to 1350 °C. The most common among the primary raw materials are arsenic, cadmium and mercury. Similar elements with their origin in many secondary raw materials, such as WEEE (waste electric and electronic equipment), are gallium, indium, tin and germanium.[77]

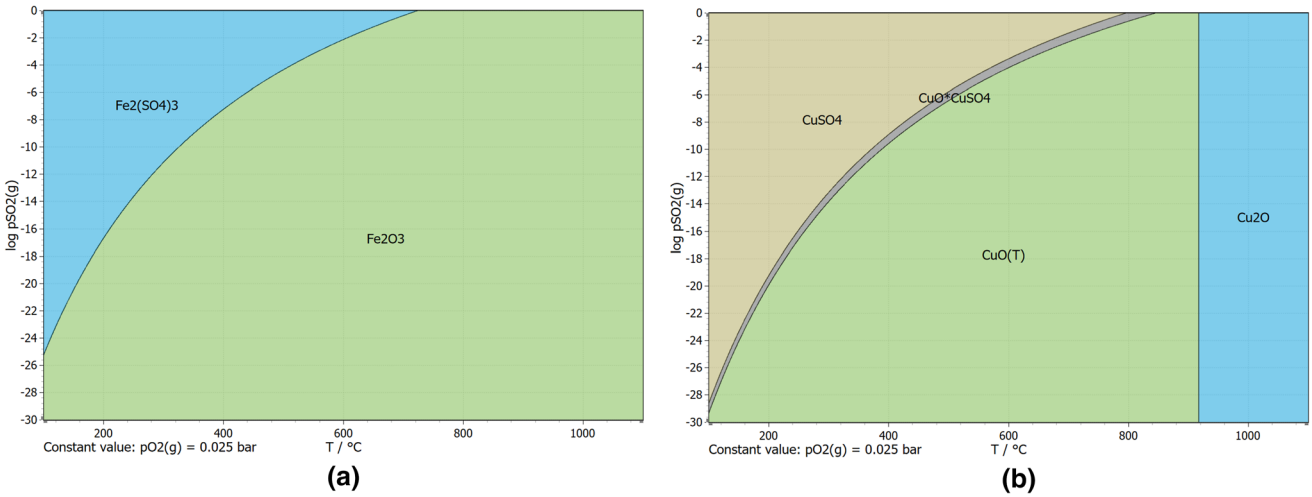


Fig. 15—The predominance area diagrams of the Fe–S–O (*a*) and Cu–S–O (*b*) systems in an atmosphere of fixed oxygen partial pressure of $p(O_2) = 0.025$ bar; the thermochemical data and graphics from HSC 9.0[81]

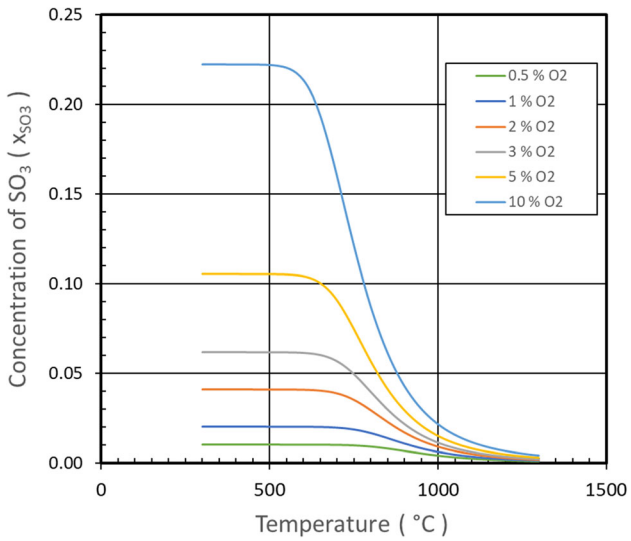


Fig. 16—The equilibrium $SO_3(g)$ pressure in various $SO_2$–$O_2(g)$ mixtures as a function of temperature; the calculations were carried out using the MTDATA software and SGTE pure substance database[41]; the concentration of oxygen in legend refers to that at 1300 °C, $p(SO_2) = 0.5$ atm.

The low melting points of oxide-sulfide systems cause stickiness in the flue dust and promote accretion growth, *e.g.*, the FeO–FeS–$Fe_3O_4$ oxysulfide melts have the lowest stability temperatures at approximately 940 °C to 950 °C[78] and copper matte droplets below 900 °C, let alone the low-iron nickel mattes which have melting points below 600 °C,[79] which are significantly lower than the off-gas temperatures entering the boiler and its radiation section[80]; see Figure 14.

For this reason, the sulfides in the flue dust are intentionally oxidized in the end of the settler and in the US by controlled addition of air or oxygen in the off-gas stream. The overall requirement for this is the controlled draught in the furnace and its settler and the off-gas train. There is no residual free sulfur in the off-gas flow entering the settler and further the US due to the strong mixing of the suspension and the dispersed nature of the sulfide combustion reactions in RS, as described above in this article. This is also one fundamental detail, different from many bath smelting technologies used for primary matte smelting[61] and also in the INCO flash smelting, which needs post-combustion for eliminating the free sulfur ($S_2(g)$) from the off-gas.

## VI. HEAT RECOVERY BOILER

The large volumetric flow rate of the off-gas in the US and the short distance between the FSF/FCF and the boiler do not allow cooling of the gas in the refractory lined uptake shaft. The dust entering the heat recovery boiler is typically at the same temperature as the slag top surface or gas in the settler. It is mixed with extra air or oxygen injected in the front end of the boiler for controlled sulfation. The heat recovery boiler (HRB) converts the enthalpy content to typically 60 bar steam and cools down the off gas of the smelting furnace down to about 350 °C, which is a typical operating temperature of the electrostatic precipitator (ESP) in the end of the smelter gas train before the main gas blower of the smelter and the acid plant.

### A. *Flue Dust Management*

Within the temperature range of the boiler, chemical reactions take place in the off-gas with the flue dust and also homogeneously in the gas phase. Their strict control is important for on-line availability of the smelter as well as for many downstream operations when blocking and accretion formation in the gas train are concerned. Among them are the recombination processes of halides, vaporized in the RS, which generate gaseous halogen acids with water vapor (*e.g.*, HCl and HBr) present in the off-gas.

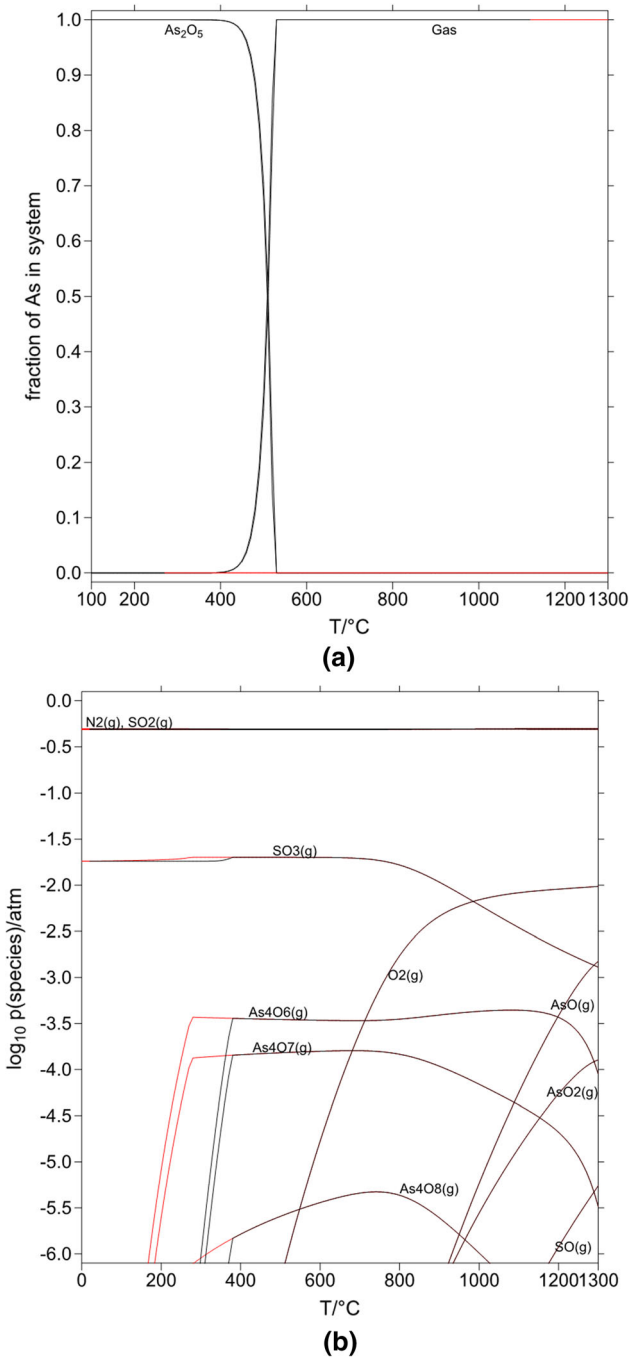


Fig. 17—(*a*) The distribution of arsenic between different phases as a function of temperature in 50 vol pct $SO_2$ FSF off-gas with 0.1, 1 and 5 vol pct $O_2$(g) at 1200 °C and 0.5 pct As in gas (calculated using MTDATA and SGTE pure substance database[41]). (*b*) Speciation equilibria of arsenic in a $SO_2$–$O_2$ atmosphere with 50 pct $SO_2$ and 1 pct $O_2$, containing 0.1 pct $As_2O_3$ at 1300 °C, during cooling to 0 °C; the 'easiest crystallizing' phase is cubic $As_2O_5$ and claudetite (monoclinic $As_2O_3$).

The purpose of adding a controlled amount of oxygen in the cooling off-gas in HRB is conversion of oxidic flue dust particles into sulfates. This improves flowability of the flue dust. Together with the absence of any sulfidic, low-melting material sulfates allow its smooth removal from the membrane tube surfaces of the boiler sections without formation of hard accretions. The build-ups slow down the heat transfer and contract the off-gas flow. The dust sulfation reactions, *e.g.*,

$$\mathrm{MeO} + {}^{1}\!/_{2}\mathrm{O_2(g)} + \mathrm{SO_2(g)} = \mathrm{MeSO_4}, \qquad [17]$$

depend on element Me, the prevailing oxygen and sulfur dioxide partial pressures as well as temperature, as shown in Figure 15.

## B. *Oxidation of $SO_2$(g) in HRB*

Sulfation of metal oxides in HRB is also a competing reaction with the formation of sulfur trioxide in the low-temperature segments of the boiler where the kinetically slow oxidation of sulfur dioxide becomes thermodynamically favorable. The oxidation takes place as a homogeneous gas reaction as

$$\mathrm{SO_2(g)} + {}^{1}\!/_{2}\mathrm{O_2(g)} = \mathrm{SO_3(g)}, \qquad [18]$$

and the equilibrium is clearly on the side of the reaction products below about 700 °C, as shown in Figure 16. The rate constant reaches its maximum at about 475 °C (750 K).[82] In the acid plant and its washing section, the formed sulfur trioxide turns into sulfuric acid ('weak acid' or 'black acid'), which contains the remaining traces of the flue dust, mostly very fine arsenic, cadmium and mercury oxides.

Many flue dust components catalyze the sulfur trioxide formation,[83,84] which makes the control of HRB chemistry and the flue dust management difficult. There, the various geometries of the HRB and its 'dead zones' with a slow gas flow rate may have an impact.[79]

The dust sulfating reactions [17] and the oxidation of sulfur dioxide [18] are strongly exothermic, and they make a significant contribution to the energy recovered in the HRB of a FSF and FCF.

Low-boiling metals, such as cadmium, mercury, zinc and arsenic,[85] exist largely as metal vapors in the RS, settler and US. Depending on their concentrations and their compounds' boiling points, vapor pressures and precipitation kinetics, they start to condense in the HRB and form the very fine fraction of the flue dust.[86] They, thus, condense as pure substances in the temperature ranges which are within the dew points of their oxides, sulfides and sometimes metals as determined by the surrounding gas phase; see Figure 17. This is the reason for the very heterogeneous mineralogy of the FSF flue dust[87] and why the individual crystals of the fine flue dust often exist as pure substances without any visible interactions with the other particles. The excess air in the off-gas train and the design of the HRB may also have an impact on the oxidation degree of, *e.g.*, arsenic in the flue dust, as shown by recent XPS (X-ray photoelectron spectroscopy) studies.[88] The trace element distributions in a copper smelter are sensitive to the internal coupling of the plant and very much dependent on how flue dust and slag concentrate are treated, *i.e.*, whether they are continuously fed back to the smelting or bled for impurity removal to another treatment circuit.[89] In the first option, their only outlets are anodes and slag,

whereas in the second option, the trace element concentrations in the smelting step (RS, settler and off-gas train) are regulated to a specific level.

## VII. ESP AND ACID PLANT

The kinetic conditions at temperatures occurring in the off-gas train post HRB are not very favorable for chemical reactions. For environmental reasons, however, it is essential that some elements and their compounds in the off-gas at temperatures < 350 °C still have significant vapor pressures which keep their total concentrations high, with reference to the allowed concentrations from the point of view of fugitive emissions and safe exposure to atmosphere. In Figure 17(b), the gaseous arsenic concentration 5 mg As/$Nm^3$ as its oxides is reached around 100 °C. Such hazardous emissions cannot be captured by bag filters or any similar dry treatment if the gas temperature is too high.

Halogens make a significant contribution to the HRB membrane walls on the corrosion phenomena of the steels,[90] which is assisted by the fact that at low boiler pressures (< 60 bar) the dew point of sulfuric acid may be passed, and formation of liquid sulfuric acid becomes possible.[91]

The final removal of impurities takes place in the gas washing department of the acid plant which captures all fumes and gaseous species provided the scrubber temperature is low enough. Some trace-level concentrations of metal vapors may remain in the gas fouling the catalytic converter where they may end up in the production acid.[92] This issue may be emphasized by increased amounts of secondary materials to be used in the future as feed stock of the primary copper smelting.[93]

## VIII. SUMMARY AND CONCLUSIONS

This review was focused on the experimental and fundamental data available in the literature on unit processes in the flash smelting and converting of sulfide minerals. The unique vessel designs of the flash smelting and flash converting furnaces exhibit specific, unmistakably localized process steps for the chemical reactions and heat transfer in different parts of the furnace-off-gas train system.

The current knowledge about the detailed unit processes taking place in the reaction shaft, accumulated in pilot- and industrial-scale operations in the 1980s and 1990s, and has enabled numerical modeling of the suspension step and the RS reaction environment during the short flight time of individual feed mixture particles. A less detailed experimental knowledge of the behavior of minority and trace elements in the reaction shaft has limited their numerical modeling, and a deeper understanding of the interactions in atmospheres and temperature ranges known to persist in the oxidation zone of the copper and nickel sulfide concentrates in RS is needed. Some conclusions for the future research, based on the general stability of the impurity sulfide minerals, are been presented in this article.

The settler processes with the oxidized feed mixture have been qualitatively described in the literature already in the early stages of the FSF and FCF technology development, but their details are still less well documented. This is due to the harsh environment and problematic location of the furnace volume where the matte and slag formation take place. This review summarized the available information and described the physical properties of the initial stages as well as the end point of the slag formation. The advanced thermodynamic tools and databases enabling calculations in multicomponent and multiphase systems have been utilized for visualizing the phase relations and activities of the species in the settler. It is obvious that the large particle size difference between the fluxing sand and sulfide concentrate leads to a low-silica pool of molten, partially oxidized feed mixture where the sulfide matte and slag gradually separate and at the same time dissolve increasing fractions of silica from the flux particles, until the final slag assay has formed. Those micro-scale processes take place in relatively high $p(SO_2)$, which is different from the bath smelting technologies. CFD simulations coupled with the chemical reactions and their heat generation allow estimation of the flow patterns, heat transfer and reaction zones in the various sections of the furnace and its off-gas train.

Based on the temperature and gas composition profiles of the off-gas train, the detailed chemistries of the heat recovery boiler and the subsequent electrostatic precipitator have been sketched and discussed, supported by the recent advanced property measurements of the flue dust sampling campaigns from industrial copper smelters.


## ACKNOWLEDGMENTS

The authors are indebted to Dr. Katri Avarmaa for her suggestions and assistance when preparing the final version of this manuscript. The CFD simulation images of the FSF RS as well as the equipment pictures provided by Metso-Outotec Oyj are greatly acknowledged.


## CONFLICT OF INTEREST

On behalf of all authors, the corresponding author states that there is no conflict of interest.


## FUNDING

Open access funding provided by Aalto University.

## REFERENCES

1. I.V. Kojo, M.A. Reuter, and M.N. Scheidema: Primary copper smelting impact. In: *Proc. EMC 2015*, vol. I. GDBM, Clausthal-Zellerfeld, 2015, pp. 77–93.
2. I.V. Kojo, A. Jokilaakso, and P. Hanniala: *JOM*, 2000, vol. 52 (2), pp. 57–61.
3. J. Gisby, P. Taskinen, J. Pihlasalo, Z. Li, M. Tyrer, J. Pearce, K. Avarmaa, P. Björklund, H. Davies, M. Korpi, S. Martin, L. Pesonen, and J. Robinson: *Metall. Mater. Trans. B*, 2017, vol. 48B (1), pp. 91–98.
4. M. Schlesinger, M. King, K. Sole, and W. Davenport: *Extractive Metallurgy of Copper*, 5th ed., Elsevier Publ. Co., Amsterdam, 2011.
5. I-H. Jung, J. Lehmann, and E. Jak: in: *Treatise on Process Metallurgy,* vol. 2, Ch. 5.3., Applications. S. Seetharaman, A. McLean, R. Guthrie and S. Sridhar, eds, Elsevier, Oxford, 2014, pp. 741–99.
6. P. Bryk, J. Ryselin, J. Honkasalo, and R. Malmström: *JOM*, 1958, vol. 10 (6), pp. 395–400.
7. A. Lange: *Erzmetall*, 1960, vol. 13 (4 & 5), pp. 151–57.
8. S. Härkki, O. Aaltonen, and T. Tuominen: *Extractive Metallurgy of Copper*, AIME, New York, 1976, pp. 55–74.
9. J. Romppanen, P. Björklund, P. Suikkanen, K. Eklund, T. Ranki, M. Lahtinen, and S. Jyrkönen: In: *COM Cu 2019 USB Proceedings*, Aug. 18–21, Vancouver, Canada. CIM/MetSoc, Montreal, 2019, paper #594836 (13 p.).
10. W.G. Davenport and E.H. Partelpoeg: *Flash Smelting. Analysis Control and Optimization*, Pergamon Press, Oxford, 1987.
11. P. Taskinen, A. Jokilaakso, D. Lindberg, and J. Xia: *Miner. Process. Extract. Metall. (TIMM C)*, 2020, vol. 129 (2), pp. 207–20.
12. Y.B. Hahn and H.Y. Sohn: *Metall. Trans. B*, 1990, vol. 21B (6), pp. 945–58.
13. Y. Kim and N. Themelis: in *The Reinhard Schuhmann International Symposium*, Colorado Springs, D. Gaskell, J. Hager, J. Hoffmann and P. Mackey, eds. TMS, Warrendale (PA), 1986, pp. 349–69.
14. T. Ahokainen, A. Jokilaakso, J. Vaarno, and J. Järvi: in *Int. Conf. CFD in Mineral & Metal Process. and Power Generation*. CSIRO, Clayton (Victoria), 1997, pp. 213–21.
15. T. Ahokainen, A. Jokilaakso, P. Taskinen, and M. Kytö: in: *Sohn Internat. Symp.*, vol. 8 (Eds. F. Kongoli & R. Reddy). TMS, Warrendale (PA), 2006, pp. 529–43.
16. C.B. Sonordal, F.R.A. Jorgensen, P.T.L. Koh, and A. Hunt: *Appl. Mathem. Modell.*, 2006, vol. 30, pp. 1310–25.
17. S.M.I. Kytö: In: *Proc. 6th Int. Flash Smelting Symposium*. Outokumpu Oy, Espoo, 1993, pp. 189–248.
18. P. Taskinen: in: *Proceedings of the 1st International Process Metallurgy Conference (IPMC 2016)*, IT Bandung, November 10–11. Am. Inst. Physics, 2017, vol. 1805, 020001, pp. 1–11; https://doi.org/10.1063/1.4974407.
19. B.J. Elliot, F.R.A. Jorgensen, and N. Kemori: in *Metall. Process. for Early Twenty-First Century* (Ed. H.Y. Sohn), San Diego (CA), Sept. 20–23. TMS, Warrendale (PA), 1994, pp. 943–62.
20. F.R. Jorgensen, F.J. Moyle, and M.W. Wadsley: in *Proc. on the Flash Reaction Processes*. D. Robertson, H. Sohn & N. Themelis, eds. Univ. Missouri Rolla, Missouri-Rolla (MO), 1988, pp. 167–89.
21. A. Jokilaakso, R. Suominen, H. Hackman, P. Taskinen, and K. Lilius: in *Proc. on the Flash Reaction Processes*, Salt Lake City, 15.- 17.06. 1988, D. Robertson, H. Sohn & N. Themelis, eds. Univ. Missouri-Rolla, Missouri-Rolla (MO), 1988, pp. 201–13.
22. T. Laurila, R. Oikari, T. Pöyhönen, P. Joutsenoja, R. Mikkola Hernberg, T. Ranki-Kilpinen, J. Järvi, and P. Taskinen: in *Copper-Cobre 2003*, vol. IV (Book 2). C. Diaz, C. Landolt, T. Utigard, eds. CIM, Montreal (Canada), 2003, pp. 317–27.
23. L. Arias, S. Torres, C. Toro, E. Balladares, R. Parra, C. Loeza, C. Villagrán, and P. Coelho: *Sensors*, 2018, vol. 18, p. 12.
24. J.T. Yli-Penttilä, E.J. Peuraniemi, A. Jokilaakso, and K.M. Riihilahti: *Mining Metall. Explor.*, 1998, vol. 15 (4), pp. 41–47.
25. J.A. Cahill and A.D. Kirshenbaum: *J. Phys. Chem.*, 1962, vol. 66 (6), pp. 1080–82.
26. V. Montenegro, H. Sano, and T. Fujisawa: *Mater. Trans.*, 2008, vol. 49 (9), pp. 2112–18.
27. A. Shook, G. Richards, and J.K. Brimacombe: *Metall. Mater. Trans. B*, 1995, vol. 26B, pp. 719–29.
28. F.R.A. Jorgensen, B.J. Elliot, P.T.L. Koh, and T.V. Nguyen: in *Flash Reaction Processes*, T.W. Davies, ed. Kluwer Academic Publishers, The Netherlands, 1995, pp. 201–38.
29. T. Hidayat, D. Shishin, S.A. Decterov, and E. Jak: *Calphad*, 2017, vol. 58, pp. 101–14.
30. J. Vaarno, J. Järvi, T. Ahokainen, T. Laurila, and P. Taskinen: in 3rd *Int. Conf. CFD in Mineral & Metal Process. and Power Generation*. CSIRO, Clayton (Victoria), 2003, pp. 147–54.
31. Y.B. Hahn and H.Y. Sohn: *Metall. Trans. B*, 1990, vol. 21B (6), pp. 959–66.
32. F.R.A. Jorgensen and P.T.L. Koh: *JOM*, 2001, vol. 53(5), pp. 16–20.
33. A. Jokilaakso, R.O. Suominen, P.A. Taskinen, and K. Lilius: *Trans. IMM,* 1991, vol. 100(2), pp. 79–90.
34. A. Jokilaakso: *A study on suspension smelting kinetics of tetrahedrite (in Finnish)*. Lic. Tech. thesis, Helsinki University of Technology, Espoo, Finland, 1988, 120 p.
35. N.E. Tuffrey, G.G. Richards, and J.K. Brimacombe: *Metall. Mater. Trans. B*, 1995, vol. 26B(5), pp. 995–70.
36. T. Hidayat, D. Shishin, E. Jak, and S.A. Decterov: *Calphad*, 2015, vol. 48, pp. 131–44.
37. R.D. Hagni and C.B. Vierrether: in *Flash Reaction Processes*, D.G.C. Robertson, H.Y. Sohn & N.J. Themelis, eds, Salt Lake City, June 15–17, 1988. Center for Pyrometallurgy, Univ. Missouri-Rolla (MO), 1988, pp. 245–62.
38. R. Suominen, A. Jokilaakso, P. Taskinen, and K. Lilius: *Scand. J. Metall.*, 1991, vol. 20 (4), pp. 245–50.
39. J. Järvi, T. Ahokainen, and A. Jokilaakso: in *Computer Applications in Metallurgy and Materials Processing*, S. Agryropoulos, M. Hasan, eds, 16–19 Aug. Calgary. The Metall. Soc. CIM, Montreal, 1998, pp. 19–29.
40. Z.S. Markovic, A. Jankovic, and R. Tomanek: *J. Min. Metall. A*, 2008, vol. 44 (1), pp. 24–30.
41. R.H. Davies, A.T. Dinsdale, J.A. Gisby, J.A.J. Robinson, and S. Martin: *Calphad*, 2002, vol. 26 (2), pp. 229–71.
42. T. Hidayat, A. Fallah-Mehrjardi, P. Hayes, and E. Jak: *Metall. Mater. Trans. B*, 2020, vol. 52B (3), pp. 963–72.
43. N. Štrbac, I. Mihajlovic, D. Minic, D. Živkovic, and Ž. Živkovic: *J. Min. Metall. B*, 2009, vol. 45(1), pp. 59–67.
44. S.M. Sadegh and J.D. Miller: *Int. J. Miner. Process.*, 2016, vol. 157, pp. 103–30.
45. P.N. Prasad, A. Lennartsson, and C. Samuelsson: *Metall. Mater. Trans. B*, 2020, vol. 51B (4), pp. 1446–59.
46. N.J. Themelis, J.K. Mäkinen, and N.D.H. Munroe: in: *Physical Chemistry of Extractive Metallurgy*, TMS, Warrendale (PA), 1985, pp. 289–309.
47. D. Shishin, T. Hidayat, E. Jak, and S. Decterov: *Calphad*, 2013, vol. 41 (1), pp. 160–79.

48. N. Kemori, Y. Ojima, and Y. Kondo: *Shigen-to-Sozai*, 1990, vol. 106 (9), pp. 545–50.
49. Y. Mori and N. Kemori: *Shigen-to-Sozai*, 1996, vol. 112 (10), pp. 723–28.
50. M. Pérez-Tello, J. Tirado-Ochoa, H. Sohn, and V. Sánchez-Corrales: *JOM*, 2002, vol. 54 (10), pp. 27–30.
51. D. Higgins, N. Gray, and M. Davidson: in *7th Int. Conf. CFD in the Minerals and Process. Ind.*, 9–11 Dec. Melbourne. CSIRO, Melbourne, 2009, 6p.
52. F.R.A. Jorgensen, R.N. Taylor, W. Dickingson, and I. Stevenson: in *Extractive Metallurgy of Gold and Base Metals*. Kalgoorlie October 26–28, 1992. The Australas. IMM, Victoria, 1992, pp. 395–400.
53. S. Härkki and J. Juusela: New Developments in Outokumpu Flash Smelting Method. A paper presented in *AIME 103rd Annual Meeting 1974*, Dallas (TX), Feb. 25–27. TMS Paper Selection, #A74–18, 1974, 20 p.
54. L. Klemettinen, K. Avarmaa, and P. Taskinen: *World Metall. Erzmetall*, 2017, vol. 70 (5), pp. 257–64.
55. R. Schuhmann: *Trans. AIME/J. Metals*, 1950, vol. 188 (7), pp. 873–84.
56. D. Shishin, P. Hayes, and E. Jak: In: *COM Cu 2019 USB Proceedings*, Aug. 18–21, Vancouver, Canada. CIM/MetSoc, Montreal, 2019, paper #594861 (12 p.).
57. K. Avarmaa, H. O'Brien, H. Johto, and P. Taskinen: *J. Sustain. Metall.*, 2015, vol. 1 (3), pp. 216–28.
58. P. Piskunen, K. Avarmaa, H. O'Brien, L. Klemettinen, H. Johto, and P. Taskinen: *Metall. Mater. Trans. B*, 2018, vol. 49B (1), pp. 98–112.
59. D. Sukhomlinov, L. Klemettinen, H. O'Brien, P. Taskinen, and A. Jokilaakso: *Metall. Mater. Trans. B*, 2019, vol. 50B (6), pp. 2723–32.
60. P. Taskinen: *Miner. Proc. Extr Metall.*, 2011, vol. 120 (4), pp. 240–46.
61. P. Coursol, P.J. Mackey, J.P.T. Kapusta, and N. Cardona Valencia: *JOM*, 2015, vol. 67 (5), pp. 1066–74.
62. J. Vaarno: *Modeling concept for intensive reacting submerged gas injection a case study of a Peirce-Smith converter*. PhD thesis, Helsinki University of Technology, Espoo (Finland), 2002, 131 p.
63. M. Chen, K. Avarmaa, L. Klemettinen, H. O'Brien, D. Sukhomlinov, J. Shi, P. Taskinen, and A. Jokilaakso: *Metall. Mater. Trans. B*, 2020, vol. 51B (4), pp. 1495–1508.
64. S. Sineva, T. Hidayat, A. Fallah-Mehrjardi, R. Starykh, P. Hayes, and E. Jak: *Miner. Process. Extr. Metall.*, 2021. https://doi.org/10.1080/25726641.2021.1919375.
65. K. Fagerlund and H. Jalkanen: *Metall. Mater. Trans. B*, 2000, vol. 31B (3), pp. 439–51.
66. T. Ahokainen and A. Jokilaakso: *Can. Metall. Quart.*, 1998, vol. 37 (3–4), pp. 275–83.
67. Y. Shiraishi, K. Ikeda, A. Tamura, and T. Saito: *Trans. JIM*, 1978, vol. 19 (5), pp. 264–74.
68. P. Chartrand and A. Pelton: *Calphad*, 1999, vol. 23 (2), pp. 219–30.
69. E. Yazhenskikh, K. Hack, and M. Müller: *Calphad*, 2011, vol. 35 (1), pp. 6–19.
70. T.A. Utlak and T.M. Bessmann: *J. Am. Ceram. Soc.*, 2018, vol. 101 (2), pp. 928–48.
71. J. Xia, T. Ahokainen, T. Kankaanpää, J. Järvi, and P. Taskinen: in *EMC 2005,* vol. 3, Sept. 18–21, Dresden. GDBH, Clausthal-Zellerfeld, Germany, 2005, pp. 1359–72.
72. J.L. Xia, T. Ahokainen, T. Kankaanpää, J. Järvi, and P. Taskinen: *Steel Res. Internat.*, 2007, vol. 78 (2), pp. 155–59.
73. J.-P. Jylhä, N. Khan, and A. Jokilaakso: *Processes*, 2020, vol. 8, #485 (17 p.).
74. J. Zhou, Z. Chen, P. Zhou, J. Yu, and A. Liu: *Trans. Nonferrous Met. Soc. China*, 2012, vol. 22, pp. 1517–25.
75. N. Khan and A. Jokilaakso: in *Extraction 2018, Proc. First Global Conf. Extract. Metall.* B.R. Davis, M.S. Moats & S. Wang, eds, Ottawa, Aug. 26–29. TMS, Warrendale (PA), 2018, pp. 993–1005.
76. P. Tan: *JOM*, 2011, vol. 63 (12), pp. 51–57.
77. K. Avarmaa, S. Yliaho, and P. Taskinen: *Waste Manage.*, 2018, vol. 71 (1), pp. 400–10.
78. H. Johto, H. Henao, E. Jak, and P. Taskinen: *Metall. Mater. Trans. B*, 2013, vol. 44B (6), pp. 1364–70.
79. K.C. Hsieh and Y.A. Chang: *Can. Metall. Q*, 1987, vol. 26(4), pp. 311–27.
80. Y. Yang, A. Jokilaakso, P. Taskinen, and M. Kytö: *JOM*, 1999, vol. 51 (5), pp. 36–40.
81. A. Roine: *HSC Chemistry, vers. 9*. Outotec Pori, 2020, (accessed in July 2020; https://www.outotec.com/products-and-services/technologies/digital-solutions/hsc-chemistry/).
82. A. Yilmaz, L. Hindiyarti, A.D. Jensen, P. Glarborg, and P. Marshall: *J. Phys. Chem. A*, 2006, vol. 110 (21), pp. 6654–59.
83. J. Lehmusto, E. Vainio, T. Laurén, and M. Lindgren: *Metall. Mater. Trans. B*, 2018, vol. 49B (1), pp. 434–39.
84. J. Lehmusto, T. Laurén, and M. Lindgren: *JOM*, 2019, vol. 71 (9), pp. 3305–13.
85. C.B. Alcock, V.P. Itkin, and M.K. Horrigan: *Can. Metall. Q.*, 1984, vol. 23 (3), pp. 309–313.
86. T. Ranki-Kilpinen: *Sulfation of cuprous and cupric oxide dusts and heterogeneous copper matte particles in simulated flash smelting heat recovery boiler conditions*. PhD thesis, Helsinki University of Technology, Espoo, 2004, 62 p.
87. E. Miettinen: *Thermal conductivity and characteristics of copper flash smelting flue dust accretions*. PhD thesis, Helsinki University of Technology, Espoo, 2008, 87 p.
88. Y. Chen, Z. Zhao, P. Taskinen, Y. Liang, H. Ouyang, B. Peng, A. Jokilaakso, S. Zhou, T. Chen, N. Peng, and H. Liu: *Metall. Mater. Trans. B*, 2020, vol. 51B (5), pp. 2596–2608.
89. M. Moats, L. Alagha, and K. Awuah-Offei: *J. Clean. Prod.* 2021, vol. 307, p. 127207.
90. H. Viitala: *Corrosion mechanisms of the heat recovery boiler of copper flash smelting*. PhD thesis, Aalto University, Espoo, 2020, 78 p. (https://aaltodoc.aalto.fi/handle/123456789/42843).
91. S. Sarkar: *JOM*, 1982, vol. 34 (10), pp. 43–47.
92. I.V. Kojo and H. Storch: In: *Sohn Internat. Symp.*, vol. 8 F. Kongoli & R. Reddy, eds, TMS, Warrendale (PA), 2006, pp. 225–38.
93. K. Avarmaa, L. Klemettinen, H. O'Brien, and P. Taskinen: *Miner. Eng.*, 2019, vol. 133, pp. 95–02.